Electronic Supplementary Material (ESI) for Nanoscale Advances.
This journal is © The Royal Society of Chemistry 2020

# Electronic Supplementary Information

## Sepiolite and pigments structures

Sepiolite is a natural mineral of chemical formula $Si_{12}Mg_8O_{30}(OH)_4(OH2)_4.8H_2O$. Volle *et al* [1] and Ovarlez *et al* [2] described in detail this material and its applications. Sepiolite is mainly used as a filler to reinforce polymers, but its particular structure gives it a large number of other possible uses (paints, buildings, cosmetics…). The unique sepiolite structure consists of continuous two-dimensional tetrahedral sheets of talc type and discontinuous octahedral sheets (see Figure S1 from Volle *et al* [1]). Thanks to these discontinuous octahedral ribbons, periodic nano-pores of rectangular section are formed within the main structure of the fibre. When these pores are on the surface of the fibre, they form channels. If the pores are embedded within the fibre, they make tunnels. Consequently, it is possible to insert molecules such as dyes inside the channels and/or tunnels to form composite materials: pigments. Note that the tunnels are naturally filled with zeolitic water under ambient conditions.

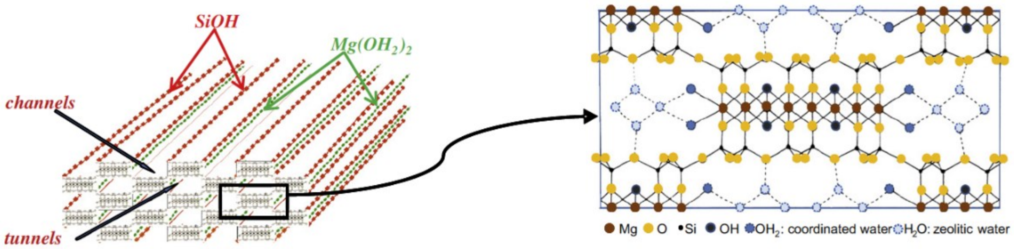

**Figure S1** : *Schematic presentation of the sepiolite fibre: the layer of silica extends as a continuous layer with inversion generating uniform size of tunnels and channels (11.5 Å-3.7 Å) along the fibre*" according to Volle *et al* [1].

The single sepiolite fibre has a typical lateral dimension of 20-30 nm and a length range of 0.5-5 µm.

When organic molecules are used with raw sepiolite, such as indigo powder to create the famous Maya Blue pigment [2], the dye is more located on the external surface of the sepiolite fibre (channels and ends of the tunnels) (see Figure S2).

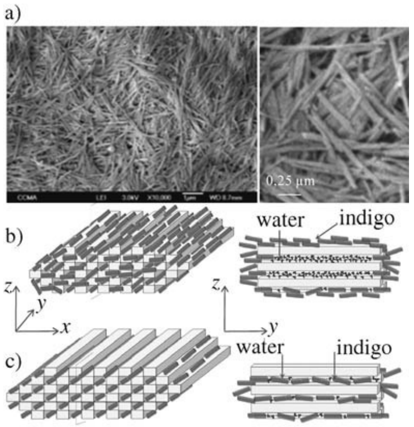

**Figure S2** : "*a) SEM image of dispersed pristine sepiolite fibres (scale bar: left = 1 mm, right = 0.25 mm); b) schematic representation of indigo/sepiolite mix in which indigo interacts with the external surface and the ends of the tunnels, and water is then blocked in internal channels; c) schematic representation of the indigo/sepiolite mix in which indigo interacts with external and internal channels, and zeolitic water is then replaced by indigo*" according to Ovarlez *et al* [2].

## Experimental details of SEM observations

In this study, we did not have the possibility of using a Transmission Electron Microscope, as was the case in the work of Dazon et al [3] for individual particle number size distribution. However, it was possible to use two Scanning Electron Microscopes, one hosted by Institut Jean Lamour (Nancy, France) and the second by the LEDNA laboratory (Saclay CEA Center, France). Table S1 summarises the sample preparation and the SEM parameters used for these observations. A minimum of 30 SEM micrographs were taken for each material and analysed for particle counting.

**Table S1** : Details of sample preparation and SEM parameters used for observations of powder mixes and determinations of individual particle size distributions. The XL30 FEG SEM belongs to the Institut Jean Lamour and the Ultra 55 Zeiss belongs to the CEA center.

| **Powder** | **Code (proportion in the mix, in wt. %)** | **SEM apparatus** | **Sample preparation** | **SEM parameter** |
|---|---|---|---|---|
| TiO$_2$ | TiO$_2$ A/ TiO$_2$ E (90/10) | XL30 FEG Philips | Dispersion of the TiO$_2$ mixes in distilled water at pH > 8/Deposition of one dispersion droplet on a target plot covered by carbon scotch/metallisation of the samples after drying in a desiccator | Magnification: 25-50k<br>Acceleration voltage: 2 kV |
| | TiO$_2$ A/ TiO$_2$ E (80/20) | | | Magnification: 25-150k<br>Acceleration voltage: 2 kV |
| | TiO$_2$ A/ TiO$_2$ E (70/30) | | | Magnification: 25-100k<br>Acceleration voltage: 2 kV |
| | TiO$_2$ A/ TiO$_2$ E (60/40) | | | Magnification 25-50k<br>Acceleration voltage: 2 kV |
| | TiO$_2$ A/ TiO$_2$ E (50/50) | | | Magnification: 25-100k<br>Acceleration voltage: 2 kV |
| Sepiolite | Sepiolite | Ultra 55 Zeiss | Raw powder deposition (a few mg) on a SEM target plot covered by carbon scotch | Magnification: 0.5-10k<br>Acceleration voltage: 1.5 kV |
| Sepiolite based pigment | B19 | | | |
| | BN 19 | | | |
| | R10 | | | |
| | J4 | | | |

## Sample preparation for nitrogen adsorption and helium pycnometry

Before nitrogen adsorption and helium pycnometry experiments, the powder samples must be outgassed to remove molecules (humidity and contamination) naturally adsorbed on the particles' surfaces. Table S2 briefly describes these outgassing conditions. Generally, for nitrogen adsorption, the samples are outgassed by combining temperature and vacuum. For sepiolite and pigments, there was a risk of material degradation under temperature and under vacuum (evolution of the water molecules from the sepiolite structure and elimination of the dye), this is why we did not heat the materials during the outgassing phase and that we operated at 60°C during helium pycnometry, a temperature for which we are sure that the materials are not degraded [1, 2]. For all TiO$_2$ powders, nitrogen adsorption at 77K (ASAP 2020, Micromeritics®) was repeated 3 times as well as helium pycnometry (Accupyc 1340, Micromeritics®). For sepiolite and pigments, nitrogen adsorption was repeated 3 times but skeletal densities were measured only once by helium pycnometry. For $TiO_2$, the $A_{Ex}$ and skeletal densities indicated in Table 2 of the manuscript with their uncertainties (one standard deviation for 3 runs) therefore correspond to average values. For sepiolite and pigments, the $A_{Ex}$ indicated are also average values with one standard deviation. Likewise, the average values of VSSA are indicated with one standard deviation.

**Table S2** : Outgassing conditions for nitrogen adsorption and helium pycnometry on powder mixes.

| Powder | Code (proportion in the mix, in wt. %) | Nitrogen adsorption outgassing (ASAP 2020 Micromeritics®) | Helium pycnometry outgassing (Laboratory oven) |
|---|---|---|---|
| $TiO_2$ | $TiO_2$ A/ $TiO_2$ E (90/10) | 24h in desorption station under secondary vacuum @ 200°C | 24 h in a laboratory oven @ 150°C |
| | $TiO_2$ A/ $TiO_2$ E (80/20) | | |
| | $TiO_2$ A/ $TiO_2$ E (70/30) | | |
| | $TiO_2$ A/ $TiO_2$ E (60/40) | | |
| | $TiO_2$ A/ $TiO_2$ E (50/50) | | |
| Sepiolite | Sepiolite | 24h in desorption station under secondary vacuum @ room temperature | 24 h in a laboratory oven @ 60°C |
| Sepiolite-based pigment | B19 | | |
| | BN 19 | | |
| | R10 | | |
| | J4 | | |

## Constituent particle size distributions of $TiO_2$ mixes, sepiolite and pigments

Figures S3 and S4 show respectively the constituent particles number size distribution for raw $TiO_2$ A and $TiO_2$ E (from Dazon *et al* [3] work). Figure S5 shows the constituent particle number size distributions obtained for the $TiO_2$ mixes based on the SEM micrographs. The image processing described in our previous work (see ESI from Dazon *et al* [3]) was used. Figure S6 shows the constituent particle number size distributions for sepiolite and pigments. We applied a log-normal law model on these number size distributions to assess the monodispersity of sepiolite and pigments. Sepiolite and pigments are indeed unimodal, whereas the $TiO_2$ mixes are characterised by bimodal distributions, which was expected according to the initial proportions considered. $TiO_2$ A has a median particle size of 138 nm and $TiO_2$ E of 7 nm [3], thus, two populations of particles are visualised and correspond to the particle sizes of each individual titanium dioxide.

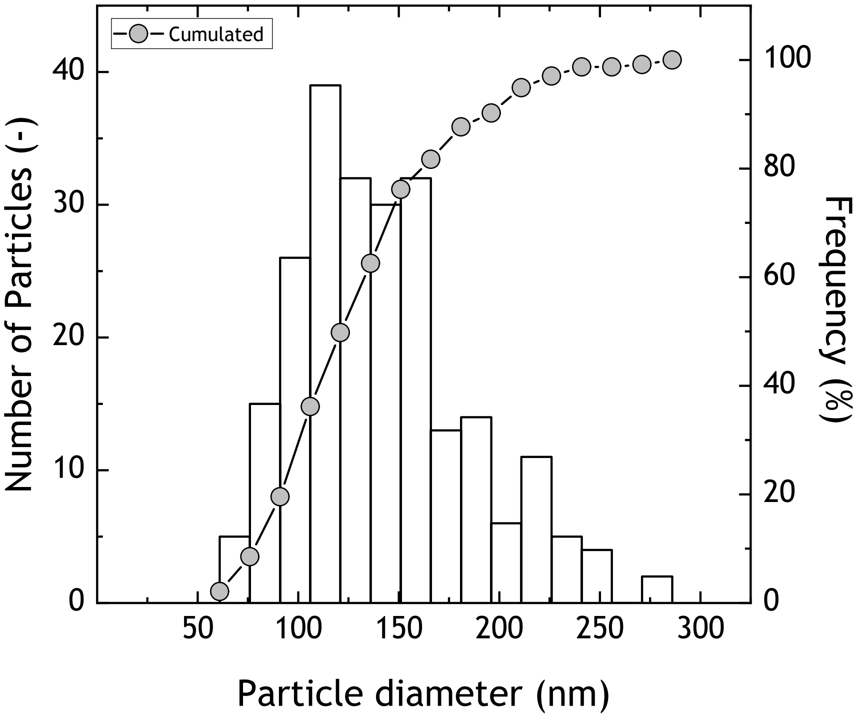

**Figure S3** : Constituent particle number size distribution of pure $TiO_2$ A (data from Dazon *et al* [3]).

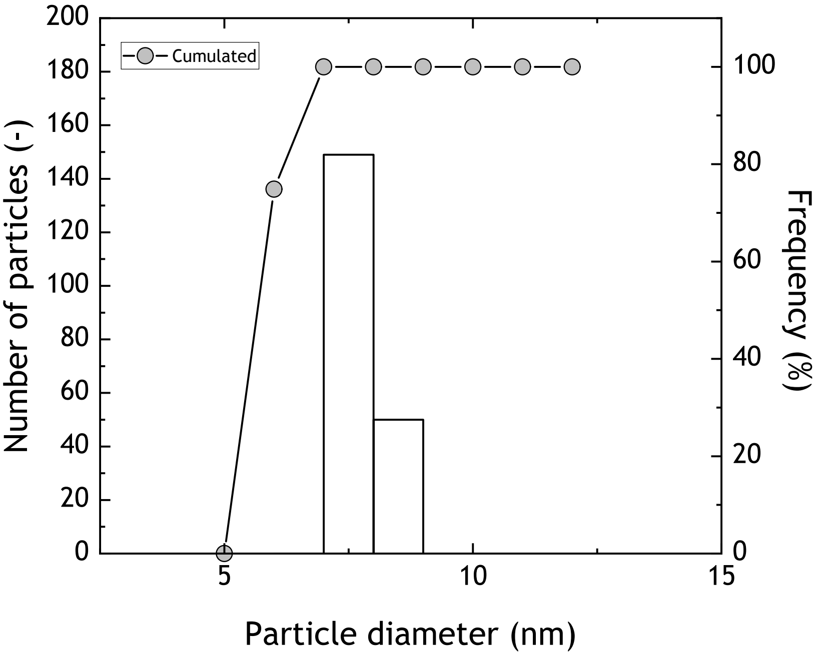

**Figure S4** : Constituent particle number size distribution of pure $TiO_2$ E (data from Dazon *et al* [3]).

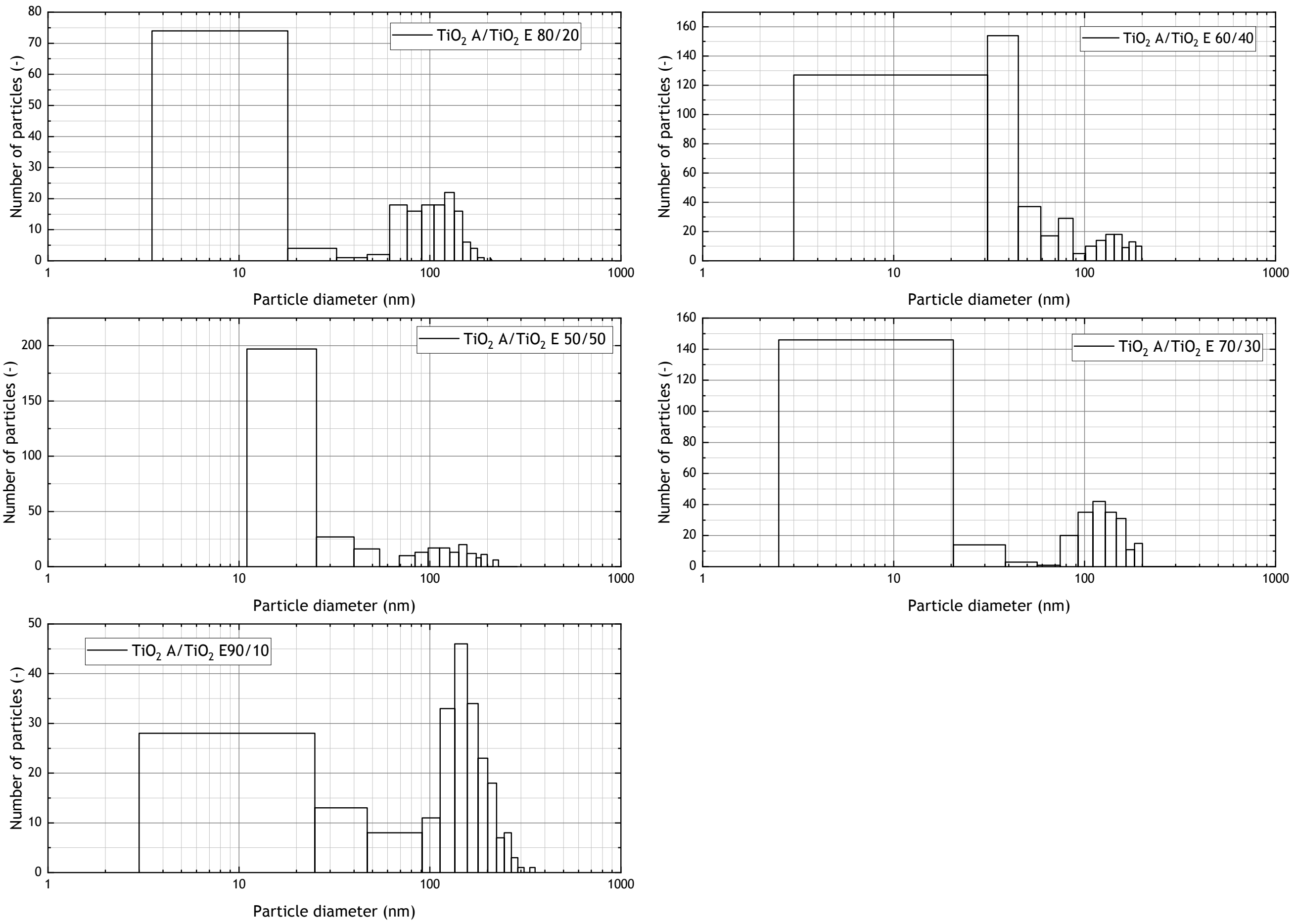

**Figure S5** : Constituent particle number size distributions of TiO$_2$ powder mixes obtained by SEM method.

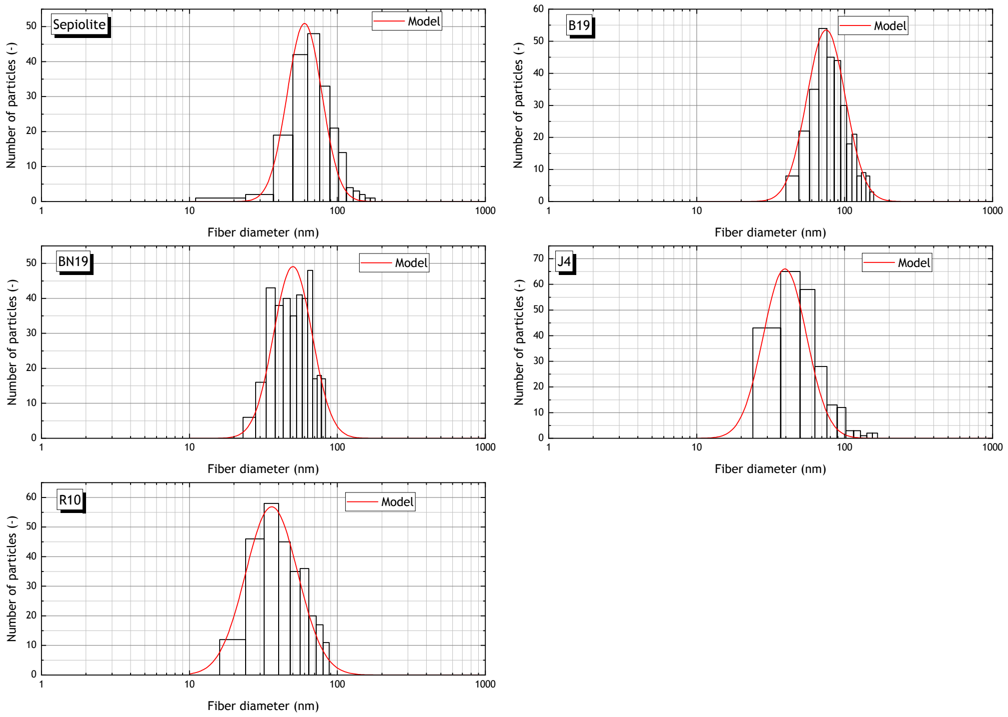

**Figure S6** : Constituent particle number size distributions of sepiolite and pigments obtained by SEM method.

## References

1 N. Volle, L. Challier, A. Burr, F. Giulieri, S. Pagnotta and AM. Chaze, *Composites Science and Technology*, 2011, **71**, 1685-1691.

2 S. Ovarlez, F. Giulieri, AM. Chaze, F. Delamare, J. Raya, and J. Hirschinger, *Chemistry: a European Journal*, 2009, **15**, 11326-11332.

3 C. Dazon, O. Witschger, S. Bau, V. Fierro and P. L. Llewellyn, *Nanoscale advances*, 2019, **1**, 3232-3242.